Vacuum 144 (2017) 152–159

Contents lists available at ScienceDirect

Vacuum

journal homepage: www.elsevier.com/locate/vacuum

Surface nanocrystallization and gradient microstructural evolutions in the surface layers of 321 stainless steel alloy treated via severe shot peening

Sadegh Pour-Ali, Ali-Reza Kiani-Rashid*, Abolfazl Babakhani

Materials and Metallurgical Engineering Department, Faculty of Engineering, Ferdowsi University of Mashhad, 91775-1111, Mashhad, Iran

ARTICLE INFO

Article history:
Received 8 July 2017
Received in revised form
16 July 2017
Accepted 17 July 2017
Available online 18 July 2017

Keywords:
321 austenitic stainless steel
Severe shot peening
Gradient microstructure evolutions
Dislocation slipping

ABSTRACT

The gradient nanocrystalline structure from the top surface to the subsurface layers of 321 austenitic stainless steel alloy was fabricated by means of severe shot peening. The microstructural evolutions including the grain size distribution and phase transformation were investigated in-depth. Experimental results showed that the dislocation slipping plays a key role in the grain refinement of this alloy and depend on the amount of imparted plastic strain, different structures including dislocation walls, dislocation tangles, mechanical twinning, lamella-shaped cells are sequentially appeared in the surface and/or subsurface grains. Due to imparting ultrahigh plastic deformation in the topmost surface, mentioned structures are converted to the nano-grains (68–82 nm) to minimize the total energy of the surface layer. In line with the grain refinement, austenite to strain induced martensite phase transformation is more affected as the plastic strain increases so that the volume fraction of latter phase reaches to 65% in the topmost surface. As a result of these evolutions, microhardness values are decreased from 281 to 120 HV in the surface layers.

1. Introduction

In recent years near-surface severe plastic deformation (NS-SPD) processes have attracted considerable attention in both of industry and academia [1]. NS-SPD processes are successful in forming the ultrafine-grains (UFGs) and nano-grains (NGs) on the surface of different classes of metallic materials including steel [2,3], aluminum [4], copper [5], nickel [6] and other alloys [7,8]. Formation of UFGs and NGs in the surface layers of mentioned metallic materials usually leads to considerable improvements in different chemical, physical, tribological and mechanical properties of mentioned materials [4]. The common feature of all NS-SPD processes is the imparting large plastic strain with high strain rates (sometimes around 10^6 s^{-1} [9]) on the surface of materials. Severe shot peening (SSP) [10,11], surface mechanical attrition treatment (SMAT) [12,13], cold rolling [14], high-frequency impacting [15], high pressure surface rolling [16], ultrasonic impact peening [17], sliding friction treatment [18,19], severe wire brushing [20], fast multiple rotaion rolling [21], and laser shock peening [22] are among the most reproducible NS-SPD processes. Based on the TEM observations, mentioned processes are common in the creation of the high dislocation density areas during the first stages of the process. After imparting further plastic deformation or higher strain rates, more dislocations are created and the structure evolution is followed by recombination and rearrangement of dislocations and afterward formation of subgrains with small and/or large misorientations in the initial grains [23].

SSP is extensively used in industry to create compressive stresses and nanocrystalline layers on the surface of different alloys. Many researchers have studied the surface nanocrystallization (SNC) via SSP during recent years. Bagherifard et al. [24] reported that nanocrystalline surface layer in cast iron via SSP improved the fatigue strength and crack initiation resistance. Wang et al. [25] produced a nanocrystallized surface layer with an average grain size of 18 nm through SSP on the 1Cr18Ni9Ti stainless steel and pointed out that the chloride induced corrosion resistance is increased after SNC. Hassani-Gangaraj et al. [26] studied the SNC of a low alloy steel and developed a model linking finite element simulation of SSP to dislocation density evolution to predict the grain size distribution in the surface layer. Zhong et al. [27] showed that SNC on the processed surface layer of iron via SSP increased the

* Corresponding author. Tel.: 00989151416718.
E-mail address: kianirashid@um.ac.ir (A.-R. Kiani-Rashid).

http://dx.doi.org/10.1016/j.vacuum.2017.07.016
0042-207X/

diffusion coefficient of Al atoms in Fe structure by 4 orders of magnitude. Jin et al. [28] predicted the strain rate distribution in commercially pure titanium treated by SSP and assessed the effect of strain rate on the SNC of CP-Ti.

The mentioned reports have focused on the nanocrystallization in the topmost surface and not illuminated the microstructure evolution in the sub-surface layers; however, in-depth microstructural evolutions during SSP can be more important than the topmost surface. In fact, this matter should be considered that after SSP and other NS-SPD processes the surface roughness is inevitably increased [29,30]. Since higher surface roughness can be led to higher stress concentration, sometimes it is needed to grind the topmost surface to obtain a smooth surface. Thus, a thick nanocrystalline layer on the bulk metallic materials with a small surface roughness will be the ideal state after SSP and/or NS-SPD processes. Hence, knowledge of the in-depth grain refinement of metallic materials during SSP processes helps in better understanding of their microstructure and performance for subsequent applications. In this paper, SSP process as a NS-SPD method was used to fabricate a gradient nanocrystalline structure on the surface of 321 stainless steel (321SS) alloy. The surface layers are analyzed by X-ray diffraction (XRD), field-emission scanning electron microscope (FE-SEM) and transmission electron microscopy (TEM). The grain refinement, phase transformation and microhardness variations are investigated in-depth.

2. Experimental procedure

The chemical composition of as-received 321SS alloy bar with a diameter of 80 mm was composed of 0.021 C, 0.557 Si, 1.485 Mn, 18.104 Cr, 0.113 Mo, 9.697 Ni, 0.016 P, 0.011 S, 0.461 Ti and balance Fe (wt.%). In order to get a homogeneous chemical composition, the bar was solution annealed in argon atmosphere at 1100 °C for 2 h. Cylindrical specimens of 6.0 mm thickness were sectioned from the bar and subjected to SSP process using an air blast apparatus (KPS SHOT Co.). For the SSP, standard high carbon steel shots (S230) with a nominal diameter of 0.58 mm and hardness of 45–50 HRC were used. SSP process was carried out by a peening nozzle with a diameter of 30 mm, mass flow rate of about 8 kg/min and air pressure of 0.30 MPa for 60 min (this condition meets a surface coverage of 1000%). To generate reproducible plastic strains, the shot angle and the distance between the nozzle and top surface were set to 90° and 400 mm, respectively.

The cross-sections of shot peened samples for FE-SEM observations were mechanically ground, polished and afterward etched in a solution containing 2.5 ml H_2O, 2.5 ml HNO_3 and 5 ml HCl. FE-SEM images were provided by a TESCAN MIRA3 field emission scanning microscope at 15 kV. The grazing incidence XRD studies were carried out using an X'Pert Pro MPD X-ray diffraction instrument operated with Cu-K_α radiation and grazing angle of 2°. Average grain size in the surface and different depths was estimated according to Williamson-Hall equation [31]:

$$\beta_r cos\theta = \left(\frac{k\lambda}{D}\right) + \mu \sin\theta \quad (1)$$

where D is the grain size, k is the Scherer's factor which is usually considered 0.9, μ is representative of strain, λ and θ are the wavelength of the irradiated x-ray and Bragg's angle, respectively. The β_r in Eq. (1) is equal to peak broadening of diffraction peaks due to SSP. In fact, β_r is equal to $\sqrt{\beta_i^2 - \beta_0^2}$, in which β_i and β_0 are full widths at half maximum (FWHM) of diffraction peaks of shot peened and non-treated sides of 321SS samples, respectively. The volume fraction of strain induced martensite (α') phase was also calculated using the following formula [32]:

$$V_{\alpha'} = \frac{(1/n)\sum_{j=1}^{n}\left(\frac{I_{\alpha'}^{j}}{R_{\alpha'}^{j}}\right)}{(1/n)\sum_{j=1}^{n}\left(\frac{I_{\gamma}^{j}}{R_{\gamma}^{j}}\right) + (1/n)\sum_{j=1}^{n}\left(\frac{I_{\alpha'}^{j}}{R_{\alpha'}^{j}}\right)} \quad (2)$$

where n, I and R are the number of peaks of the phase used in the calculation, the integrated intensity of the reflecting planes and the material scattering factor, respectively. Based on the XRD results, only two phases in each sample were considered for calculations. In-depth grain refinement of the treated samples was also characterized by transmission electron microscopy (TEM) and selected area electron diffraction (SAED) methods (Tecnai G2 operating at 200 kV). For XRD examination, shot peened 321SS samples were polished from the treated surface to reach to the given depths (≈40 μm, ≈80 μm, ≈120 μm and ≈160 μm below the shot peened surface) and then the grazing incidence XRD test was run. The thickness of samples was regularly measured by a screw thread micrometer. After XRD analysis, the untreated surface of these samples was ground and polished to get an overall thickness of about 50 μm, afterward prepared foils were perforated by dimpling and ion-milled for TEM microscopy. For each depth, five samples were considered to study the microstructure at a certain depth. It is worthy to note that for high depths (e.g. more than 150 μm [26]) which the grain refinement/microstructure evolution is not considerable, it is difficult to use TEM because of the relatively coarse grains and correspondingly limited view of the relevant structural scales, which are coarser than the TEM observations. So, in these cases FE-SEM was applied to evaluate the microstructure. In-depth microhardness measurements were also done by a Buehler microhardness tester at a load of 20 g and dwell time of 10 s. In order to eliminate the probable effect of each indentation on the microhardness values of neighboring ones, microhardness measurement was done by a certain procedure in which the distance between two neighboring indentations was above 30 μm and the vertical distance between indentation point and topmost surface was measured via optical microscope [33].

3. Results and discussion

3.1. The microstructure prior to SSP

Fig. 1 shows the microstructure characteristics of 321SS alloy prior to SSP. Considering the chemical composition of 321SS alloy especially Ni and Mn contents (austenite stabilizer elements) and Fig. 1a and b, the microstructure consists of γ grains (austenite) as matrix phase and α' phase (strain induced martensite) as fine needles inside of γ grains. According to Eq. (2), $V_{\alpha'}$ value is about 10% which in turn shows that the austenite is the main phase in the solution annealed 321SS alloy. As can be seen from Fig. 1c, there is only few dislocation lines in the coarse γ grains of 321SS alloy and corresponding SAED pattern reveals that there is no remarkable misorientation in the γ grains and they are approximately perfect FCC crystals. The grain size distribution of primary γ phase measured by microstructural image processing (MIP) software has been shown in Fig. 1d. It can be seen that the average grain size of primary γ phase is about 380 μm.

3.2. Surface roughness

Fig. 2 shows the surface roughness profile and surface roughness values of severely shot peened 321SS obtained by non-contact

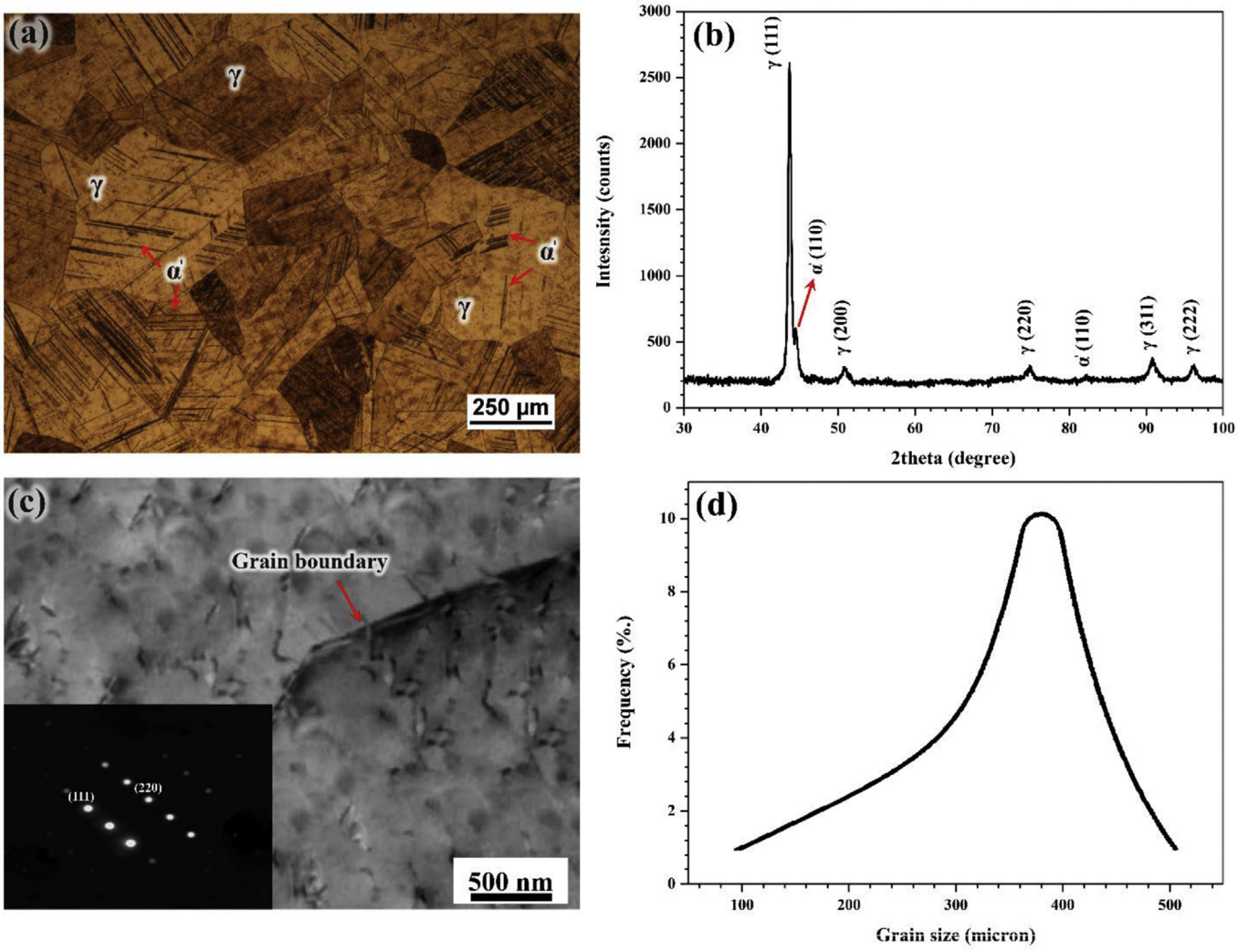

Fig. 1. (a) The original microstructure of 321SS alloy before SSP and (b) corresponding XRD pattern, (c) The bright field TEM image of primary γ phase and corresponding SAED pattern shown as the inset, (d) The grain size distribution of the γ phase after solution annealing.

3D optical profilometer. The surface roughness values are not as high as [2,34]. Some researchers stated that surface roughness increases as the coverage (plastic strain) increases [11]; however, it can be claimed that for high coverages, surface roughness is lower than low coverage ones. In fact, in the initial stages of shot peening, due to local deformation, surface roughness and surface heterogeneity remarkably increase but after over peening (high coverages), due to enhanced work hardening of surface layers, surface roughness decreases and the surface homogeneity increases. This argument is in full agreement with [35].

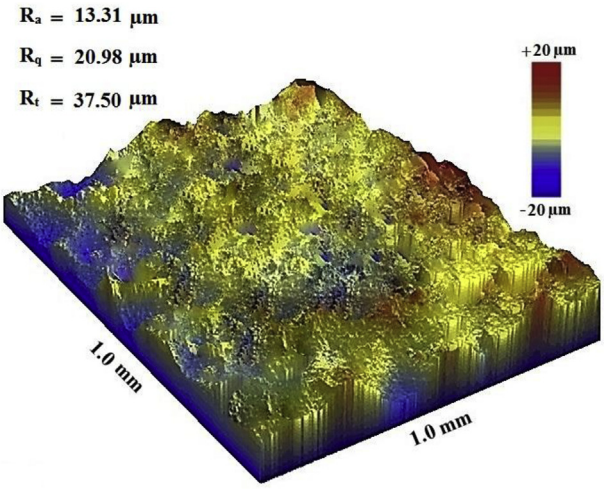

Fig. 2. Surface topography and surface roughness values of severely shot peened 321SS.

3.3. XRD analysis after SSP

Fig. 3 shows the XRD patterns at different depths from the topmost surface to matrix of 321SS after SSP. These patterns can be studied from two different points of view: (i) transformation of existing phases and (ii) peak broadening after SSP. As can be seen from Fig. 3, with approaching the top surface layer new diffraction peaks of α' (200), α' (211) and α' (220) are gradually appeared and intensified. In this way, $V_{\alpha'}$ values at 160-, 120-, 80-, 40-μm depths and the top surface are 11%, 23%, 39%, 48% and 65%, respectively. On the other hand, comparing the XRD patterns at different depths reveals the broadening in diffraction peaks in near top surface layers (up to 120 μm below top surface). The smaller the treated layer depth is, the larger the peak broadening degree, which in turn

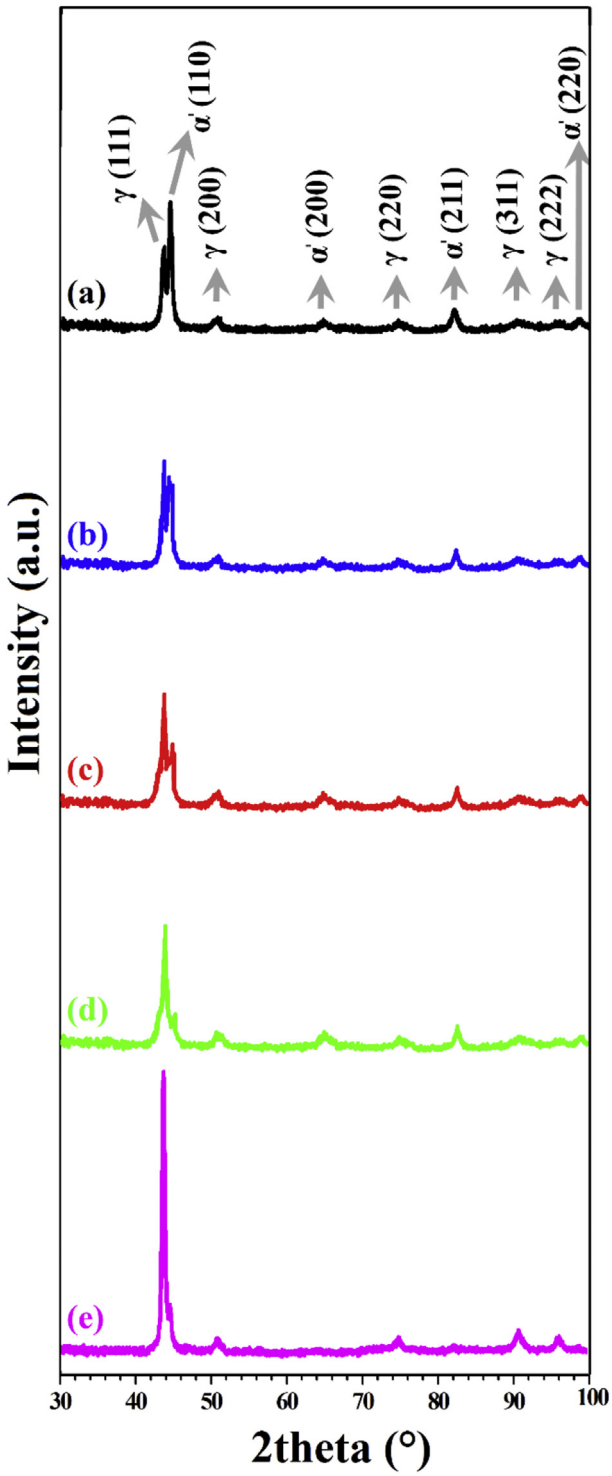

Fig. 3. XRD patterns at different depths of severe shot peened sample: (a) topmost surface and (b) ≈ 40 μm, (c) ≈ 80 μm, (d) ≈ 120 μm and (e) ≈ 160 μm below the top surface.

implied that the grain refinement degree decreased with the increasing of treated layer depth. According to equasion (1) this broadenign can be mainly attributed to the grain refinement and an increase in microstrain. The results of the Williamson-Hall analysis of the top surface of treated sample are presented in Fig. 4. In this way, the average surface grain size of the treated 321SS sample is calculated to be 53 nm. Thus, based on XRD analysis it can be claimed that the γ → α' phase transformation in the surface and subsurface layers of 321SS alloy will be severely affected by increasing the imparted plastic strain. In addition, these results clearly verify the formation of UFGs and NGs on the surface and subsurface layers of the severely shot peened 321SS alloy.

3.4. SEM and TEM analyses after SSP

Fig. 5 displays the typical SEM images of the cross-section of severe shot peened 321SS alloy. As can be seen from high magnification images, the microstructure difference between the deformation affected zone (not well-defined) and the matrix (similar to Fig. 1a) is completely distinct; however, there is not a sharp boundary between them. The total thickness of the deformation affected layer is about 120 μm which is much more bigger than that of reported for LSP [36] and SMAT [37] of austenitic stainless steels. To methodically investigate the in-depth microstructure evolutions, high magnification SEM and TEM observations at different depths were conducted (Fig. 6.). As can be seen from Fig. 6a, A nearly full SNC is obtained on the surface of treated sample so that equiaxed NGs with randomly crystallographic orientation and mean size of 75 nm are obseved in the whole of microsture. This value is larger than the XRD result. In fact, the crystallite size obtained by XRD analysis is defined as the size of the coherently scattering domains, consequently XRD can distinguish the subgrains with small misorientations and give the average size of subgrains; However, the conventional TEM imaging provides the average size of the grains with higher angle grain boundaries. This microstructural refinement is also reflected in the SAED pattrern shown in Fig. 6a, where the continous rings are appeared. Considering the proper lattice parameters (a_{γ} = 3.575 A°, $a_{\alpha'}$ = 2.868 A°), observed diffraction rings can be directly assigned to both γ and α' phases (Fig. 6a). Similar observations have also been reported for comparable surface treatments [38,39]. TEM images, including bright field (BF) image and corresponding SAED pattern at about 40 μm below the topmost surface, are shown in Fig. 6b. The main microstructural feature at this depth is the formation of lamella-shaped cells. As is obvious from Fig. 6b, the boundaries of these cells are not as straight as those of the mechanical twins and a lot of dislocation pile-ups are observed in these boundaries. The corresponding SAED pattern (imperfect rings) also exhibits a microstructural evolution and transition to coarser grains compared with the NGs on the surface. The microstructure at about 80 μm deep from the top surface is characterized by the formation of large dislocation tangles and local mechanical twining inside large elongated lamellas (see Fig. 6c). In this depth, streak spots in the SAED pattern, demonstrate that the elongated lamella are subdivided by the dislocation interactions. These results are in good agreement with the report by Roland et al. [40] dealing with the SMAT of 316 austenitic stainless steel. As can be seen from Fig. 6d, TEM image and corresponding SAED pattern of treated surface at about 120-μm depth, density of dislocations has been significantly decreased compared with shallower depths. A nearly refined microstructure is retained and some dislocation walls and dislocation tangles are observed at this depth which are piling up near the grain boundaries. In the case of about 160-μm depth, the density of dislocations compared with lower depths has been remarkably decreased (see Fig. 6e). In addition, corresponding SAED pattern also confirms that the nearly perfect crystals distributed in the whole of microstructure. As can be seen from Fig. 6f, as one moves toward deeper zones the microstructure of 321SS in the solution-annealed state is gradually appeared.

Based on the experimental data and numerical calculations, the plastic strain is decreased from the top treated surface toward deeper layers with a trend dependent on the material and intensity

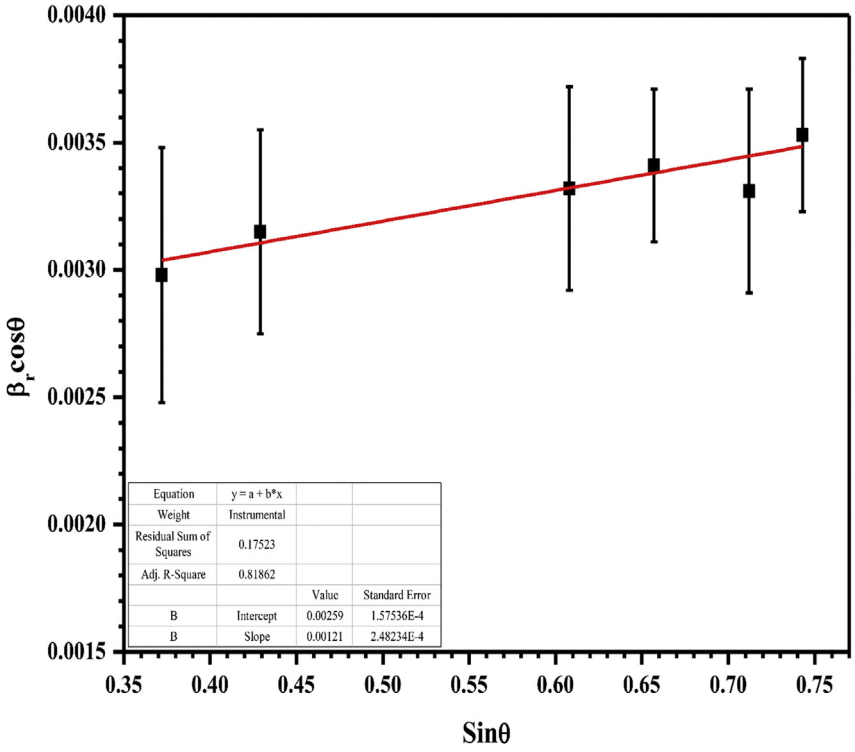

Fig. 4. Williamson-Hall analysis from the surface of severe shot peened sample.

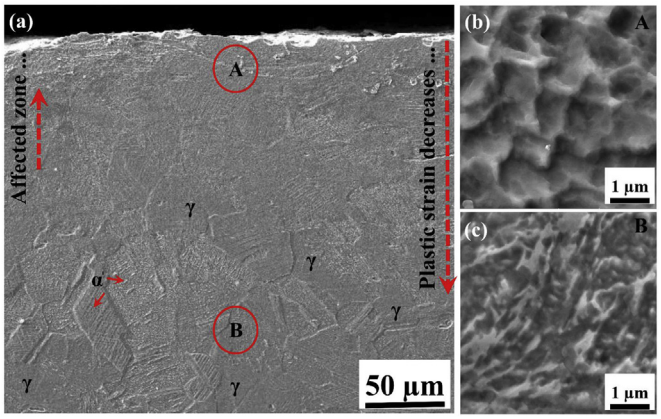

Fig. 5. (a) Cross-sectional morphology of the severe shot peened 321SS alloy and high-magnification images from (b) deformation affected zone and (c) matrix of 321SS alloy.

of SSP (imparted plastic strain) [26]. Thus, by considering the results of XRD and TEM analyses for different depths which experienced different levels of plastic strains, it is reasonable to present a sequence for the grain refinement in terms of imparted plastic strain. In this way, Fig. 7 generalizes physical mechanism of grain refinement in the surface layers of severe shot peened 321SS alloy. First of all, the slip systems are activated and density of dislocations are gradually increased. With the continuous increase in the plastic strain, density of dislocations are increased and some duplex and triplex structures containing dislocation tangles, dislocation walls and mechanical twinning are gradually appeared. Formation of mechanical twinning can help to further plastic deformation; however, their contribution is not as considerable as dislocation slipping. With the progression of plastic strain, in addition to densification of dislocation structures, original grains are subdivided into subgrains with elongated dislocation tangles and lamella-shaped cells. In the final step for ultrahigh strains, formation of NGs is only way to minimize the total energy of the system. In these conditions, equiaxed NGs (68–82 nm) are observed over the whole of microstructure (Fig. 6a). Thus, according to the amount of introduced plastic strain to each grain, it will experience a fraction or whole of mentioned evolutions. For instance in the case of zones below than 120 μm from the topmost surface, only the first step of grain refinement, activation of slip systems, is occurred. On the other hand, in the case of topmost surface, a complete microstructure evolution from the slipping activation to formation of NGs can be observed. In addition to in-depth grain refinement, based on the SAED and XRD patterns in line with this phenomenon from the top surface to subsurface layers, the $\gamma \rightarrow \alpha'$ phase transformation is also occurred. Since, the formation of α' phase is completely influenced by the amount of imparted plastic strain, it can be claimed that the $V_{\alpha'}$ values experience similar sequence.

3.5. In-depth microhardness variations after SSP

Microhardness variations with the depth from the topmost surface to the matrix of severe shot peened sample of 321SS alloy is shown in Fig. 8. The value of each data point is the arithmetic mean value of at least three single indentations at the same depth, and the error bars show the mean standard deviations. As can be seen, the top surface possesses the highest microhardness and with moving away from the top surface this parameter is gradually decreased and finally reaches to the matrix hardness. Although the average hardness of the 321SS alloy before SSP is about 120 HV (solution annealed state), this value at a depth of about 10 μm is increased by 134% after SSP. By comparing the electron microscopy images/XRD data and microhardness results in different depths, it can be stated that with higher plastic strains (i.e. lower depths), higher microhardness and finer grains are simultaneously obtained. This fact can be studied in the terms of Hall-Petch

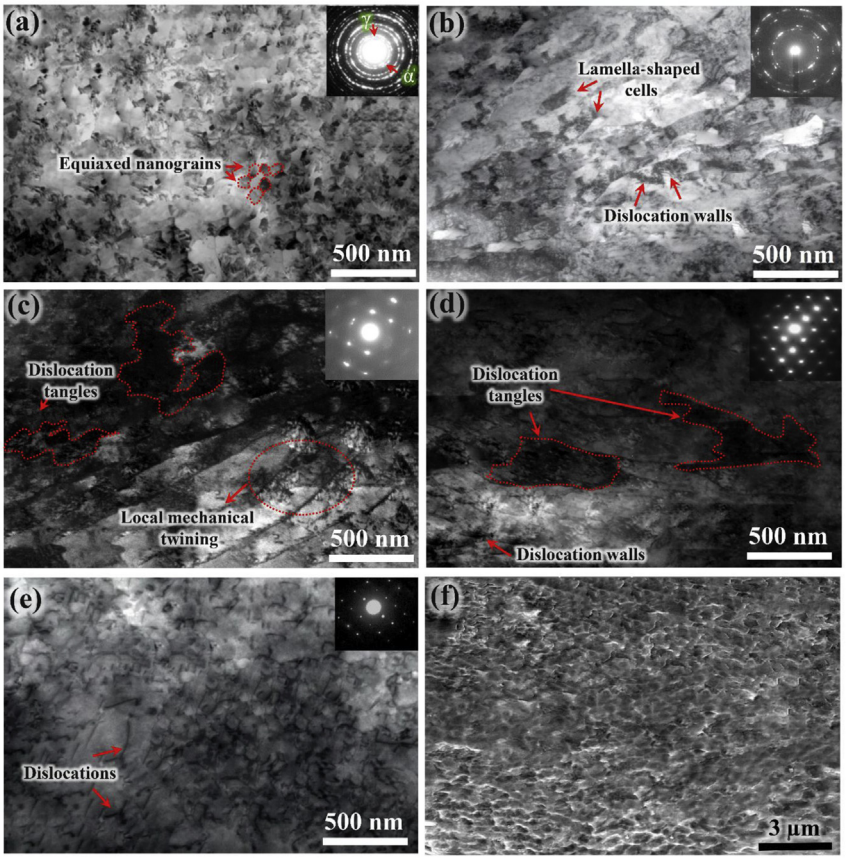

Fig. 6. Bright field TEM (a–e) and SEM (f) micrographs taken from: (a) topmost surface and (b) about 40 μm, (c) about 80 μm, (d) about 120 μm, (e) about 160 μm and (f) about 200 μm below the top surface of severe shot peened sample.

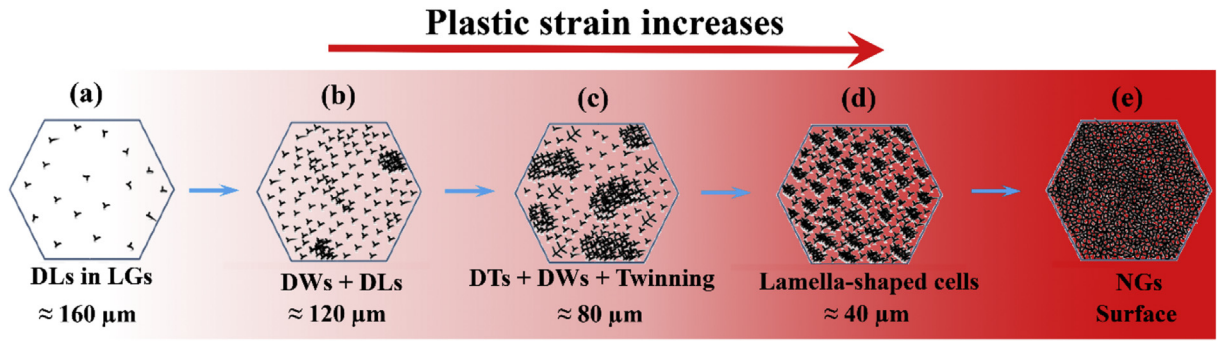

Fig. 7. Schematic diagram of the in-depth microscopic structure of the severe shot peened 321SS alloy.

relationship [41] i.e. larger reduction in grain size is reflected in an increase of the hardness. On the hand, both TEM and XRD results showed that the higher strains promote the $\gamma \rightarrow \alpha$' transformation which in turn can increase the microhardness of 321SS alloy. Thus, observed variations in the microhardness can be attributed to a certain level of grain refinement and α' phase induced by SSP impacts.

4. Conclusion

In this work, in-depth microstructural evolutions during SSP were assessed by means of XRD, SEM, TEM and microhardness tester. The main conclusions are drawn as follows.

(1) A gradient nanocrystalline microstructure with the grain size increasing from nanometer-scale to initial grain size was successfully fabricated on the surface layers of 321SS alloy by means of SSP.
(2) With increasing the amount of imparted plastic strain, from the subsurface layers to the topmost surface, degree of microstructural evolutions (grain refinement and $\gamma \rightarrow \alpha$' transformation) are increased. In fact, according to the amount of imparted plastic strain to a given grain, different structures including dislocation walls, dislocation tangles, mechanical twinning, lamella-shaped cells and finally NGs are sequentially appeared.

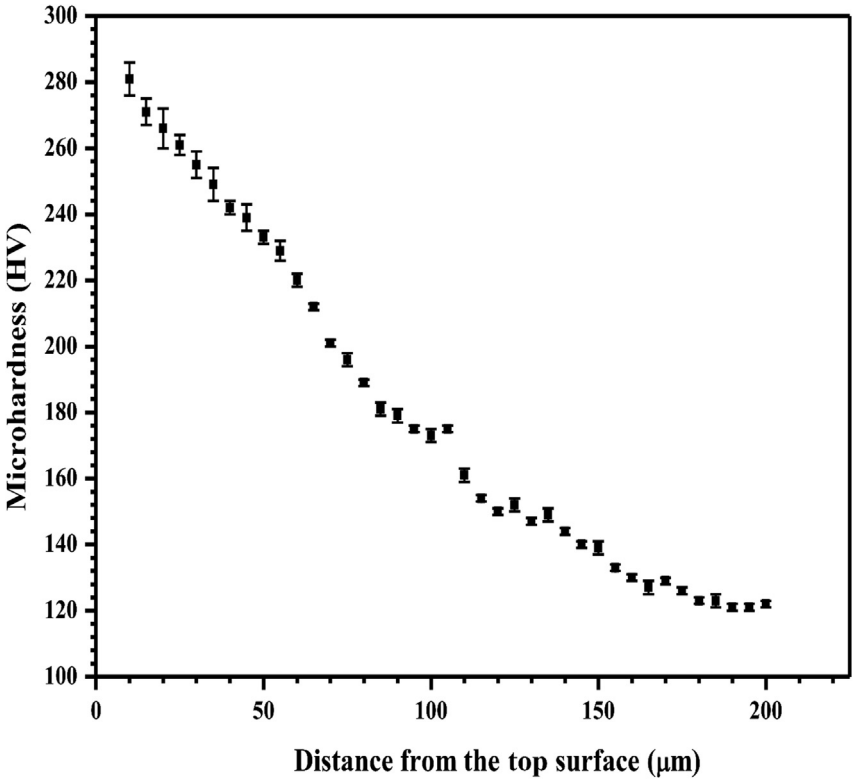

Fig. 8. Variations of microhardness with the depth in the severe shot peened 321SS alloy.

(3) Both of dislocation slipping and deformation twinning have contributed in the NS-SPD induced by SSP; however, the role of deformation twinning is nearly negligible.
(4) The average grain size of the surface of treated sample measured by XRD and TEM analyses are 53 and 75 nm, respectively.
(5) The microhardness from the 10 μm below the top surface to the matrix of treated 321SS alloy gradiently decreases from 281 to 120 HV (by 134%). These variations are attributed to the amount of grain refinement and α' formation.

Acknowledgements

Authors would like to appreciate the financial support from the Ferdowsi University of Mashhad (FUM, Iran) (324-5408). Mr. Mohsen Noroozi (College of Mechanics and Materials, Hohai University) is acknowledged for his collaboration in TEM. The authors also thank Mr. Sina Hejazi, Dr. Saeed Abbasizadeh, Mr. Ramin Dallal-Moghaddam, Mr. Hashem Teimourinejad and Mr. Afshin Nazarnejatizadeh for valuable discussions.

References

[1] M. Sato, N. Tsuji, Y. Minamino, Y. Koizumi, Formation of nanocrystalline surface layers in various metallic materials by near surface severe plastic deformation, Sci. Technol. Adv. Mater 5 (2004) 145–152, http://dx.doi.org/10.1016/j.stam.2003.10.015.
[2] S. Bagherifard, S. Slawik, I. Fernández-Pariente, C. Pauly, F. Mücklich, M. Guagliano, Nanoscale surface modification of AISI 316L stainless steel by severe shot peening, Mater. Des. 102 (2016) 68–77, http://dx.doi.org/10.1016/j.matdes.2016.03.162.
[3] Z. Cheng, D. Song, J. Jiang, J. Jiang, X. Ma, K. You, A. MA, Microstructure characteristic and electrochemical corrosion behavior of surface nanocrystallization modified carbon steel, J. Iron Steel Res. Int. 23 (2016) 1281–1289, http://dx.doi.org/10.1016/S1006-706X(16)30189-3.
[4] N.A. Prakash, R. Gnanamoorthy, M. Kamaraj, Surface nanocrystallization of aluminium alloy by controlled ball impact technique, Surf. Coatings Technol. 210 (2012) 78–89, http://dx.doi.org/10.1016/j.surfcoat.2012.08.069.
[5] X.Y. Mao, D.Y. Li, F. Fang, R.S. Tan, J.Q. Jiang, Application of a simple surface nanocrystallization process to a Cu–30Ni alloy for enhanced resistances to wear and corrosive wear, Wear 271 (2011) 1224–1230, http://dx.doi.org/10.1016/j.wear.2010.12.063.
[6] J.C. Villegas, L.L. Shaw, Nanocrystallization process and mechanism in a nickel alloy subjected to surface severe plastic deformation, Acta Mater 57 (2009) 5782–5795, http://dx.doi.org/10.1016/j.actamat.2009.08.005.
[7] X.D. Ren, J.J. Huang, W.F. Zhou, S.D. Xu, F.F. Liu, Surface nano-crystallization of AZ91D magnesium alloy induced by laser shock processing, Mater. Des. 86 (2015) 421–426, http://dx.doi.org/10.1016/j.matdes.2015.07.039.
[8] H. Gao, W. Chen, Z. Zhang, Evolution Mechanism of Surface Nanocrystallization of Tungsten-copper Alloys, 2016, http://dx.doi.org/10.1016/j.matlet.2016.04.104.
[9] E. Nordin, K. Ekström, B. Alfredsson, Experimental investigation of the strain rate dependence of the SS 2506 gear steel, in: Int. Conf. Shot Peen, 2014.
[10] S. Dai, Y. Zhu, Z. Huang, Microstructure evolution and strengthening mechanisms of pure titanium with nano-structured surface obtained by high energy shot peening, Vacuum 125 (2016) 215–221, http://dx.doi.org/10.1016/j.vacuum.2016.01.001.
[11] O. Unal, A. Cahit Karaoglanli, R. Varol, A. Kobayashi, Microstructure evolution and mechanical behavior of severe shot peened commercially pure titanium, Vacuum 110 (2014) 202–206, http://dx.doi.org/10.1016/j.vacuum.2014.08.004.
[12] L. Zhang, Y. Zou, H. Wang, L. Meng, J. Liu, Z. Zhang, Surface nanocrystallization of Mg-3wt.% Li-6wt.% Al alloy by surface mechanical attrition treatment, Mater. Charact. 120 (2016) 124–128, http://dx.doi.org/10.1016/j.matchar.2016.08.017.
[13] Q. Yao, J. Sun, G. Zhang, W. Tong, H. Zhang, Enhanced toughness of nitrided layers formed on Ti-6Al-4V alloy via surface mechanical attrition pre-treatment, Vacuum 142 (2017) 45–51, http://dx.doi.org/10.1016/j.vacuum.2017.05.004.
[14] V. Demers, V. Brailovski, S.D. Prokoshkin, K.E. Inaekyan, Optimization of the cold rolling processing for continuous manufacturing of nanostructured Ti–Ni shape memory alloys, J. Mater. Process. Technol. 209 (2009) 3096–3105, http://dx.doi.org/10.1016/j.jmatprotec.2008.07.016.
[15] X. Zhao, C. Chen, F. Chen, Effect of the Precipitated Phase of MgZn2 on Surface Nanocrystallization of Al-zn-Mg Alloy Based on High-frequency Impacting and Rolling, 2017, http://dx.doi.org/10.1016/j.matlet.2016.11.107.
[16] M. Liu, J.Y. Li, Y. Ma, T.Y. Yuan, Q.S. Mei, Surface nanocrystallization and property of Ti6Al4V alloy induced by high pressure surface rolling, Surf. Coatings Technol. 289 (2016) 94–100, http://dx.doi.org/10.1016/j.surfcoat.2016.01.043.

[17] B.N. Mordyuk, O.P. Karasevskaya, G.I. Prokopenko, N.I. Khripta, Ultrafine-grained textured surface layer on Zr–1%Nb alloy produced by ultrasonic impact peening for enhanced corrosion resistance, Surf. Coatings Technol. 210 (2012) 54–61, http://dx.doi.org/10.1016/j.surfcoat.2012.08.063.
[18] W. Zhang, Q. Wei, W.T. Huo, J.W. Lu, J.J. Hu, Y.S. Zhang, Dynamic recrystallization in nanocrystalline AZ31 Mg-alloy, Vacuum 143 (2017) 236–240, http://dx.doi.org/10.1016/j.vacuum.2017.06.023.
[19] W. Zhang, W.T. Huo, J.W. Lu, J.J. Hu, Q. Wei, Y.S. Zhang, Gradient shear banding in a magnesium alloy induced by sliding friction treatment, Vacuum (2017), http://dx.doi.org/10.1016/j.vacuum.2017.05.035.
[20] S. Pour-Ali, A. Kiani-Rashid, A. Babakhani, Improved corrosion inhibition of 3-amino-1, 2, 4-triazole on mild steel electrode in HCl solution using surface nanocrystallization, Int. J. Mater. Res. 107 (2016) 1031–1040.
[21] Y. Li, K. Sun, P. Liu, Y. Liu, P. Chui, Surface nanocrystallization induced by fast multiple rotation rolling on Ti-6Al-4V and its effect on microstructure and properties, Vacuum 101 (2014) 102–106, http://dx.doi.org/10.1016/j.vacuum.2013.07.028.
[22] L. Zhou, W. He, S. Luo, C. Long, C. Wang, X. Nie, G. He, X. Shen, Y. Li, Laser shock peening induced surface nanocrystallization and martensite transformation in austenitic stainless steel, J. Alloys Compd. 655 (2016) 66–70, http://dx.doi.org/10.1016/j.jallcom.2015.06.268.
[23] O. Unal, R. Varol, Almen intensity effect on microstructure and mechanical properties of low carbon steel subjected to severe shot peening, Appl. Surf. Sci. 290 (2014) 40–47, http://dx.doi.org/10.1016/j.apsusc.2013.10.184.
[24] S. Bagherifard, I. Fernandez-Pariente, R. Ghelichi, M. Guagliano, Effect of severe shot peening on microstructure and fatigue strength of cast iron, Int. J. Fatigue 65 (2014) 64–70, http://dx.doi.org/10.1016/j.ijfatigue.2013.08.022.
[25] T. Wang, J. Yu, B. Dong, Surface nanocrystallization induced by shot peening and its effect on corrosion resistance of 1Cr18Ni9Ti stainless steel, Surf. Coatings Technol. 200 (2006) 4777–4781, http://dx.doi.org/10.1016/j.surfcoat.2005.04.046.
[26] S.M. Hassani-Gangaraj, K.S. Cho, H.-J.L. Voigt, M. Guagliano, C.A. Schuh, Experimental assessment and simulation of surface nanocrystallization by severe shot peening, Acta Mater 97 (2015) 105–115, http://dx.doi.org/10.1016/j.actamat.2015.06.054.
[27] C. Zhong, L. Liu, Y. Wu, Y. Deng, B. Shen, B. Shu, W. Hu, Diffusion Behavior of Aluminum in the Surface Layer of Iron Processed by Shot Peening, 2010, http://dx.doi.org/10.1016/j.matlet.2010.03.046.
[28] C. Jin, C. Chen, G. Li, Study on the plastic strain rate and its effect on surface nanocrystallization during shot peening, J. Comput. Theor. Nanosci. 9 (2012) 1333–1336.
[29] Y.G. Liu, M.Q. Li, H.J. Liu, Nanostructure and surface roughness in the processed surface layer of Ti-6Al-4V via shot peening, Mater. Charact. 123 (2017) 83–90, http://dx.doi.org/10.1016/j.matchar.2016.11.020.
[30] L. Zhu, Y. Guan, Y. Wang, Z. Xie, J. Lin, J. Zhai, Influence of process parameters of ultrasonic shot peening on surface roughness and hydrophilicity of pure titanium, Surf. Coatings Technol. 317 (2017) 38–53, http://dx.doi.org/10.1016/j.surfcoat.2017.03.044.
[31] S. Pour-Ali, A. Kiani-Rashid, A. Babakhani, A. Davoodi, Enhanced protective properties of epoxy/polyaniline-camphorsulfonate nanocomposite coating on an ultrafine-grained metallic surface, Appl. Surf. Sci. 376 (2016) 121–132, http://dx.doi.org/10.1016/j.apsusc.2016.03.131.
[32] A.K. De, D.C. Murdock, M.C. Mataya, J.G. Speer, D.K. Matlock, Quantitative measurement of deformation-induced martensite in 304 stainless steel by X-ray diffraction, Scr. Mater 50 (2004) 1445–1449, http://dx.doi.org/10.1016/j.scriptamat.2004.03.011.
[33] H. Li, Y. Liu, M. Li, H. Liu, The gradient crystalline structure and microhardness in the treated layer of TC17 via high energy shot peening, Appl. Surf. Sci. 357 (2015) 197–203, http://dx.doi.org/10.1016/j.apsusc.2015.09.013.
[34] S. Bagherifard, I. Fernandez-Pariente, R. Ghelichi, M. Guagliano, Effect of severe shot peening on microstructure and fatigue strength of cast iron, Int. J. Fatigue 65 (2014) 64–70, http://dx.doi.org/10.1016/j.ijfatigue.2013.08.022.
[35] V. Azar, B. Hashemi, M. Rezaee Yazdi, The effect of shot peening on fatigue and corrosion behavior of 316L stainless steel in Ringer's solution, Surf. Coatings Technol. 204 (2010) 3546–3551, http://dx.doi.org/10.1016/j.surfcoat.2010.04.015.
[36] Q. Lu, Q. Su, F. Wang, C. Zhang, Y. Lu, M. Nastasi, B. Cui, Influence of laser shock peening on irradiation defects in austenitic stainless steels, J. Nucl. Mater 489 (2017) 203–210, http://dx.doi.org/10.1016/j.jnucmat.2017.03.046.
[37] S. Bahl, S. Suwas, T. Ungàr, K. Chatterjee, Elucidating microstructural evolution and strengthening mechanisms in nanocrystalline surface induced by surface mechanical attrition treatment of stainless steel, Acta Mater 122 (2017) 138–151, http://dx.doi.org/10.1016/j.actamat.2016.09.041.
[38] N.R. Tao, Z.B. Wang, W.P. Tong, M.L. Sui, J. Lu, K. Lu, An investigation of surface nanocrystallization mechanism in Fe induced by surface mechanical attrition treatment, Acta Mater 50 (2002) 4603–4616, http://dx.doi.org/10.1016/S1359-6454(02)00310-5.
[39] G. Liu, J. Lu, K. Lu, Surface nanocrystallization of 316L stainless steel induced by ultrasonic shot peening, Mater. Sci. Eng. A 286 (2000) 91–95, http://dx.doi.org/10.1016/S0921-5093(00)00686-9.
[40] T. Roland, D. Retraint, K. Lu, J. Lu, Enhanced mechanical behavior of a nanocrystallised stainless steel and its thermal stability, Mater. Sci. Eng. A 445 (2007) 281–288, http://dx.doi.org/10.1016/j.msea.2006.09.041.
[41] X.H. Chen, J. Lu, L. Lu, K. Lu, Tensile properties of a nanocrystalline 316L austenitic stainless steel, Scr. Mater 52 (2005) 1039–1044, http://dx.doi.org/10.1016/j.scriptamat.2005.01.023.